

The Effect of Bedding Laminations  
on Crack Propagation in the  
Marcellus Shale

Evan McMullen

Advisor: Wen-lu Zhu

April 26<sup>th</sup>, 2013

Geology 394

## Table of Contents

Table of Contents.....	2
Abstract.....	3
Introduction.....	4
2. Objectives of Research.....	5
1 Hypothesis.....	5
3. Experimental Design.....	6
1. Sample Description.....	6
2. Undeformed Porosity and Permeability.....	7
3. Sample Preparations.....	7
4. Deformation.....	8
5. Porosity and Permeability of Deformed Samples & Microstructure Analysis.....	9
4. Experimental Results and Analysis of Uncertainty.....	9
1. Undeformed Porosity and Permeability.....	9
2. Mechanical Data.....	10
3. Porosity and Permeability of Deformed Samples.....	11
4. Microstructure Analysis.....	12
5. Uncertainty.....	13
5. Discussion.....	13
1. Undeformed Samples.....	13
2. Deformation Experiments.....	14
3. Deformed Samples.....	17
4. Microstructure Analysis.....	18
Future Work.....	24
Conclusion.....	24
Acknowledgements.....	25
References.....	26
Appendix.....	28
A) Figures.....	28
B) Equations.....	31
C) Tables.....	32
C) Honor Code.....	35

## **Abstract**

Natural gas extraction from shale has been increasing over the past two decades due to the novel applications of technical innovations. In order for the gas to be released, the shale layer must be fractured. The preferred method of extracting the gas is hydraulic fracturing (fracking) of rock layers. This process involves pumping water, sand, and solvents into the shale, and the pressurized fluid creates crack networks that allow oil and gas to flow. Shale is a fine-grained clastic sedimentary rock with thin laminations parallel to its bedding. To better understand the propagation of cracks through this anisotropic rock, it is important to consider the effect of laminations on crack growth. In this study I conducted deformation experiments on three Marcellus Shale samples, to investigate the effect of laminations on crack propagation. Cylindrical samples were used in the mechanical test. Two of the samples were taken parallel to the bedding planes (i.e. bedding parallel), and one was taken perpendicular to the bedding planes (i.e. bedding perpendicular). Prior to the deformation tests, initial porosity and permeability of the undeformed samples were measured. The deformation tests were conducted at room temperature. At the confinements and strain rates used in the study, all three samples failed by brittle fractures. Porosity and permeability measurements were then conducted on the deformed samples. By mechanically fracturing the samples, permeability and crack networks have been enhanced due to the internal features of the shale. I also performed microstructural analysis of undeformed and deformed samples. Comparison of the mechanical data and microstructure of bedding parallel to bedding perpendicular samples supports my hypothesis that the bedding orientation relative to stress orientation affects crack propagation. I also observed that crack growth is not only affected by the thin laminations, but also the strength contrast between silt-sized particles and clay minerals in these Marcellus Shale samples.

## Introduction

The Marcellus Shale is an economically important formation that is under constant debate due to perceived environmental issues (Olmstead et al., 2013). The Marcellus formation was deposited in the Appalachian basin during the middle Devonian time period. Over time, the organic-rich mud was buried creating the Marcellus shale. The real extent of the formation is over 124,319 square kilometers, occurring primarily in the subsurface of Pennsylvania, Ohio, New York, Maryland, Virginia and West Virginia (NETL, 2010). The thickness of the Marcellus shale varies from east to west with the average thickness being around 100 feet thick. The formation consists mainly of black shale, several lighter color shales, and small limestone layers scattered throughout the formation. The Onondago Limestone underlies the Marcellus and the Tully Limestone overlies it NETL (2010). The limestone surrounding the formation creates a stratigraphic trap, preventing natural gas from escaping the shale layer. The shale is a fine grained sedimentary rock consisting of silt-sized quartz, dolomite and calcite, pyrite, illiite-rich clay minerals, and organic matter. Subparallel to bedding planes, black cracks filled in with small silt sized particles define the anisotropic layers of the shale. Clay matter is a secondary feature to the shale and seen randomly oriented within the laminations (seen in Fig. 1).

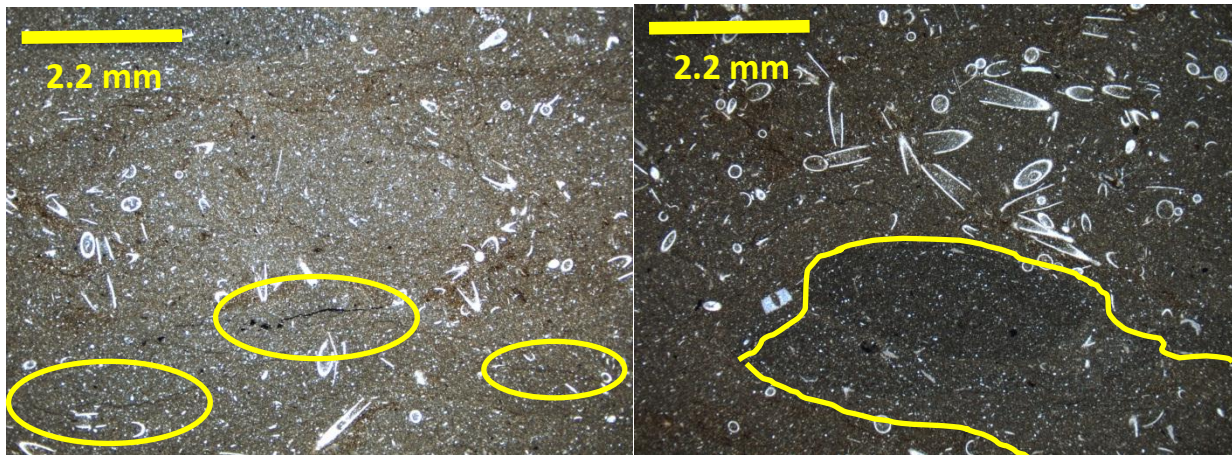


Figure 1: Left: thin section view of an undeformed Marcellus Shale sample. Circled in yellow are black cracks subparallel to bedding planes. Right: micro-fossils randomly scattered throughout the thin section view with yellow outline showing clay matter randomly oriented within laminations.

Previous studies on shales investigate the shear strength properties associated with core samples. This was accomplished by taking samples in 15 degree increments in the range of 0 to 90 degrees from the original bedding orientation. Each sample was then subjected to stress until failure occurred. The results acquired only showed variations of observed peak strength as a function of orientation (Crawford et al., 2012). Understanding how shale cracks under stress is important to the process of extracting natural gas held in the rocks pores. This research involves gaining an understanding on how cracks propagate throughout samples of the Marcellus Shale. Small samples were taken out at different angles relative to sedimentary bedding from a Marcellus Shale core. Each cylindrical samples length is around 3.825mm and a width around

1.845mm (Fig. 2c). Bedding angle relative to the maximum stress of the core varies among samples. Conducting these deformation experiments has enabled an investigation on how bedding laminations affect crack propagation in shale rock.

## **2. Objective of Research**

Analyses of Marcellus Shale samples subjected to deformation allow us to determine how crack networks are created based on bedding orientations. Examination of deformed thin section samples to undeformed thin sections show evidence on whether bedding laminations affect rock internal characteristics. This work is significant because it allows us to focus research on one defined direction while changing the sample's bedding orientations. By taking samples at different angles relative to bedding orientation, we are able to see how a shale sample deforms while stress is applied in one defined direction. Deep underground hydraulic fracturing pressurizes shale in all directions. By focusing in on a single direction of stress, we can determine the optimal angle at which cracks will grow.

### **2.1 Hypotheses**

My first hypothesis for this research is that the laminations and bedding planes would affect some of the rock's properties such as shear strength, permeability and pre-existing planes of weakness. Shear strength is the maximum amount of stress the shale can allow before failure begins to occur. Pre-existing planes of weakness are internal defects that can lead to failure. I further hypothesize that bedding orientation will affect the crack network creation in the shale, meaning that cracks would form along possible planes of weakness. The null hypothesis for this research was that the laminations and bedding planes would not affect the rock properties nor crack growth in the shale. If deformed thin sections show evidence for cracks along bedding planes, then my hypothesis will pass.

### 3. Experimental Design

#### 3.1 Sample Description

A four-inch diameter core sample of the Marcellus shale was procured from an ongoing graduate research project. The drill core is from a well in Pennsylvania and was taken at a depth of 1,928 meters. This core is from a proprietary well, so its specific details are not allowed to be released without approval from the drilling company. The shale sample will be referred to from here on as S11. Before conducting any experiments, a few assumptions must be stated. The first assumption is that pore spaces in the shale were pre-existing and the second that the initial core was taken perpendicularly to bedding of the Marcellus shale formation.

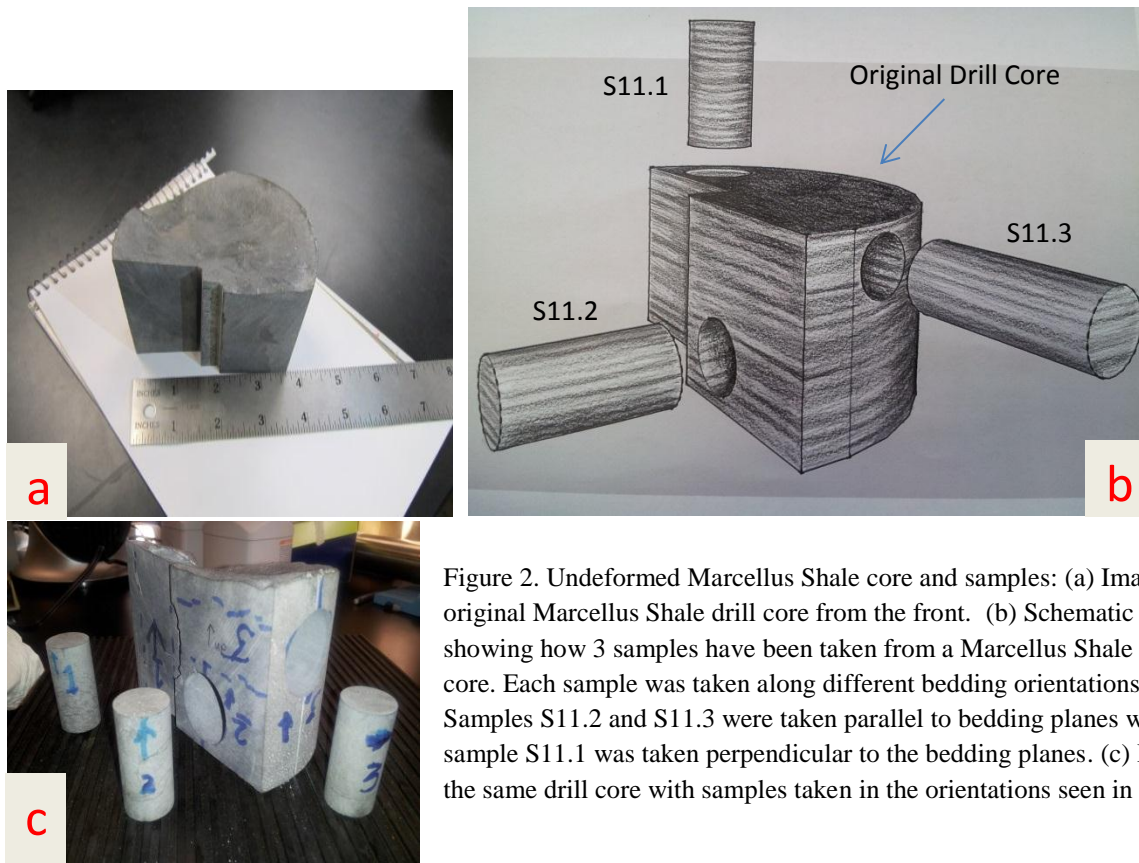


Figure 2. Undeformed Marcellus Shale core and samples: (a) Image of the original Marcellus Shale drill core from the front. (b) Schematic diagram showing how 3 samples have been taken from a Marcellus Shale drill core. Each sample was taken along different bedding orientations. Samples S11.2 and S11.3 were taken parallel to bedding planes while sample S11.1 was taken perpendicular to the bedding planes. (c) Image of the same drill core with samples taken in the orientations seen in (b).

The first task completed was the taking of a 6 mm wide slab of shale from the S11 drill core for pre-deformed shale thin sections to be made. The slab was split into three sections and sent away to the National Petrographic Lab where two thin sections were made. After carefully documenting the size and color characteristics of the large core sample (Fig. 1a), a schematic diagram of the core was created (Fig. 1b). Using the schematic diagram, the best locations for smaller samples to be drilled were determined. Once the samples locations were decided upon, the core was sent to MIT, where three samples were created. After the samples were received, they were weighed and measured for precise individual length and width (Appendix A, Fig. D-

F). Two samples were taken parallel to the expected bedding planes 90 degrees opposite of one another and a third was taken vertical to the expected bedding plane (Fig 1c).

### **3.2 Undeformed Porosity and Permeability**

The first test done on the samples was the initial porosity and permeability test. This was completed by using the porosimeter and permeameter in the Rock Physics Lab (Appendix A, Fig. A). The samples were inserted into a rubber jacket to fit into the loading chamber (Appendix A, Fig. B) tightly, preventing any gas from leaking during the test. The experimental design of the initial experiment involved testing the permeability at different confining pressures. The initial test measurement was done at a confining pressure of 2.1 MPa. With the sample length and width, the data acquisition program (Winperm) uses Darcy's Law (Appendix B, equation 2) to determine the permeability of the sample by passing nitrogen through the sample. After seven tests had been made, the confining pressure was increased by .3 MPa, and seven more tests were completed. This process continued until tests were completed at a confining pressure of ~3.1 MPa was reached. The same process was done for porosity, but the gas was changed to helium and the change in volume determines porosity. The same procedure as testing permeability was used in collecting the porosity data for the samples. Data were obtained using the porosimeter, which runs the data acquisition program (Winpor) that uses the ideal gas law (Appendix 2, equation 1) to calculate porosity values. By knowing the volume of the sample and adding a known volume of gas, percent porosity was able to be determined.

### **3.3 Sample Preparations**

After the initial porosity and permeability measurements had been made, the samples were ready to be run in the tri-axial deformation apparatus (Appendix A, Fig. C). With a limited number of samples, careful preparations were done before the samples were placed in the AutoLab 1500. The first step in preparing the sample was to cut a 0.127 mm copper sheet to surround the rim of the sample, leaving a small part of sample showing on the top and bottom. After tightly clamping the copper around the sample with rubber bands, solder was used along the gap to create a tight seal. The next step was to attach the strain gages to the copper jacket. The purpose of the strain gages is to see how the sample is deforming during the experiment. Strain gages work by having a known electrical resistance in the small foil wires. As a sample deforms, the gage deforms with it, changing the foil length and electrical resistance. This electrical resistance can be converted into strain percent that correlates to sample widening or shortening. The gages were centered on the copper shell so that they can measure any horizontal and vertical deformation during the test. A low-temperature epoxy was then applied to the back of the strain gages followed by tightly pressing the gages onto the copper to get a good seal. After the epoxy sets overnight, wires that attach to the AutoLab 1500 computer sensors to the sample are soldered onto the strain gages. This allows the computer to record any resistance change in the gages while the sample is deformed. Before the sample is ready to be put into the AutoLab 1500, a heat shrink casing and two rubber holding cells are applied to the outside of the

copper jacket to prevent confining pressure oil from entering the sample. At this point, the sample was completely prepared and ready to be run (Appendix A, Fig. G-J). Before placing the sample into the pressurizing chamber, a check to make sure the strain gages are recording data is done. This step is important because the strain gages are the only way to know what is going on inside the apparatus as well as how the rock is deforming. Once all initial checks were completed, the sample was loaded into the chamber.

### **3.4 Deformation**

All of the experiments were conducted at room temperature. For the test of sample S11.3 (seen in Fig.1b), a confining pressure of 30 MPa was used. The confining pressure corresponds to the effective overburden at the depth of where the original core was taken. For the remaining samples, S11.2 and S11.1 (Fig. 1b), a confining pressure of 15 MPa was used, allowing more brittle deformation to be induced. To start the deformation, a confining pressure of 30/15 MPa was introduced over a forty minute period. Once the confining pressure was reached, axial stress was applied. A hydraulic ram then applied a stress in the axial direction at a strain rate of  $1 \times 10^{-6}$ /s for the 30 MPa confining pressure test and a strain rate of  $5 \times 10^{-6}$ /s for the 15 MPa confining pressure test.

To better understand results acquired from the AutoLab 1500, a common plot taken during deformation will be described. As seen in Fig. 4a, there are four primary stages of the brittle failure process as stress is applied. The first stage involves crack closure, which is seen from zero stress/ zero strain and gradually begins to slope upward. This process is seen until the line becomes linear. This is stage two, which represents the samples linear elastic behavior. At any point during this stage, if stress is released, the sample will return to its original form. An increase in strain percent represents sample shortening along the axis, while decreasing strain percent represents sample expansion in the respective axis direction. In the third stage, strain percent increases at an increasing rate, which means that the sample is beginning to shorten more rapidly. This stage shows the inelastic characteristics of the sample and means that small cracks are beginning to form in the sample. The final stage is that of complete failure. This stage represents all the micro cracks formed in stage three are joining, causing faults in the sample. If stress is not stopped, complete failure will eventually occur.

For my experiments, in order to take deformed sample measurements, the occurrence of complete failure is not ideal. With increasing axial stress, brittle fractures in the sample will gradually occur. When peak stress was reached, the sample had begun to fail by fractures being developed. At this point, axial stress was stopped and gradually decreased. After the system was depressurized and empty of confining fluid, the sample was removed from the apparatus.



### **3.5 Porosity and Permeability of Deformed Samples & Microstructure Analysis**

Once the sample was removed and cleaned of all hydraulic fluids, the copper jacket was visually inspected for faults or failures. With the copper jacket still on, the final porosity and permeability tests were done and the same procedures used in the initial porosimeter and permeameter measurements were then repeated. The one difference was that after six tests at ~3.1 MPa were conducted, the confining pressure was decreased by 0.3 MPa, and six tests were done again as confining pressure was unloaded. This procedure was done until the confining pressure returned to 2.1 MPa. The reason for this design was to see how increasing, and then immediately decreasing the confining pressure around the shale affected permeability results. The only addition to final permeability data were the measurements that were taken as the sample was unloaded. After all measurements were completed, the S11.2 and S11.1 samples were wrapped and sent to the National Petrographic Lab where deformed thin sections were made perpendicular to the axis of the most visibly fractured joints. The thin sections then allowed visual understanding on how laminations affect crack growth.

## **4. Experimental Results and Analysis of Uncertainty**

### **4.1 Undeformed Porosity and Permeability**

Data were obtained from three parts of the experimental process. The initial porosity and permeability of the undeformed shale was the first to be done. Shale is known to have a very low porosity and permeability as stated in EOS (2010). Using the previously stated experimental method in section 3.2, porosity and permeability measurements were taken. With the low permeability of the carbonate-rich shale, no data was able to be acquired because the permeability was lower than what the machine can test for, which is 0.01 mD. One millidarcy (mD) is the equivalent to  $1 \times 10^{-15} \text{ m}^2$ . As for porosity, samples S11.1 and S11.2 were able to be measured. As seen in Fig. 1b, the S11.1 sample was taken perpendicular to bedding planes while the S11.2 sample was taken parallel to bedding planes. As expected, the results yielded low porosity measurements (seen in Fig. 3). Both samples showed an undeformed porosity percent between 0.1 and 0.4. For any plots or graphs in this paper, S11.1 data is represented by the color blue, S11.2 data by the color red, and S11.3 data by the color orange.

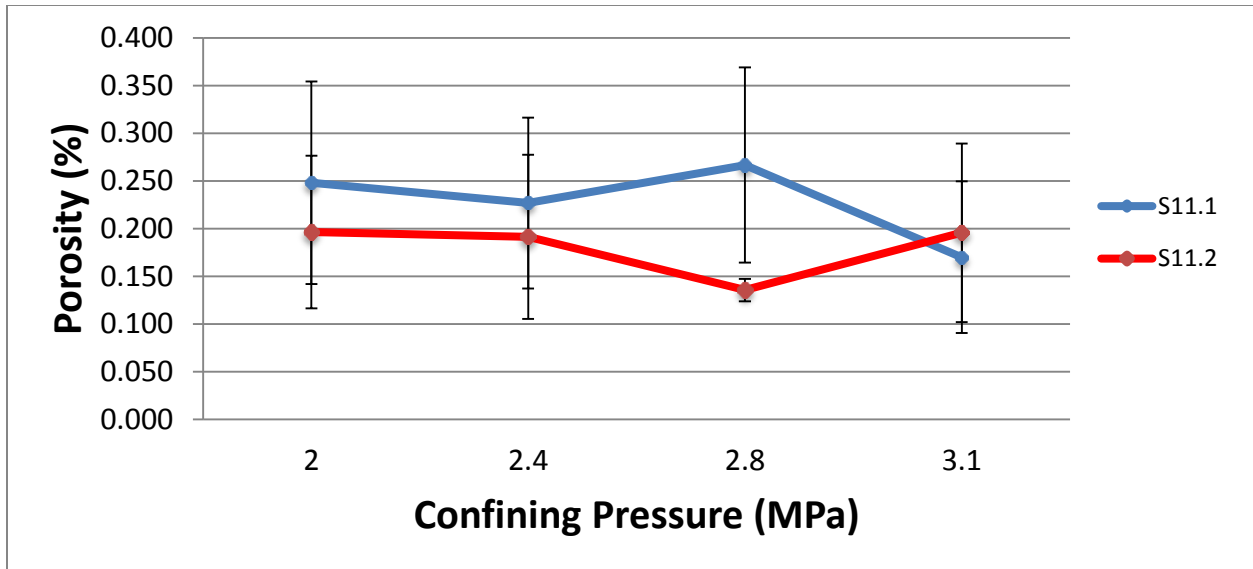


Figure 3. Undeformed sample porosity results: This graph displays the results for samples S11.1 and S11.2. S11.3 is not displayed due to the machines lower limits of measuring porosity percent. Sample S11.1 was taken perpendicular to bedding while S11.2 was taken parallel to bedding as. Error bars measure within one standard deviation.

#### 4.2 Mechanical Data

The acquired deformation results have been analyzed and plotted in Fig 4. Fig. 4b-d show data acquired during the deformation and have been plotted on a stress strain graph. Axial strain is acquired data, which is recorded by the strain gage that was attached to the sample. Volumetric strain is a calculated value which represents the deformation of the entire sample. This is calculated by adding the axial strain to two times the radial strain (Appendix B, Equation 4). This equation is derived from the basic volumetric equation. Peak stress for each sample is seen by the arrow at the top of the curve. The samples that were taken parallel to bedding planes had maximum principle stress applied along the parallel laminations. As for the sample taken perpendicularly to bedding planes, maximum principle stress was applied perpendicular to the laminations.

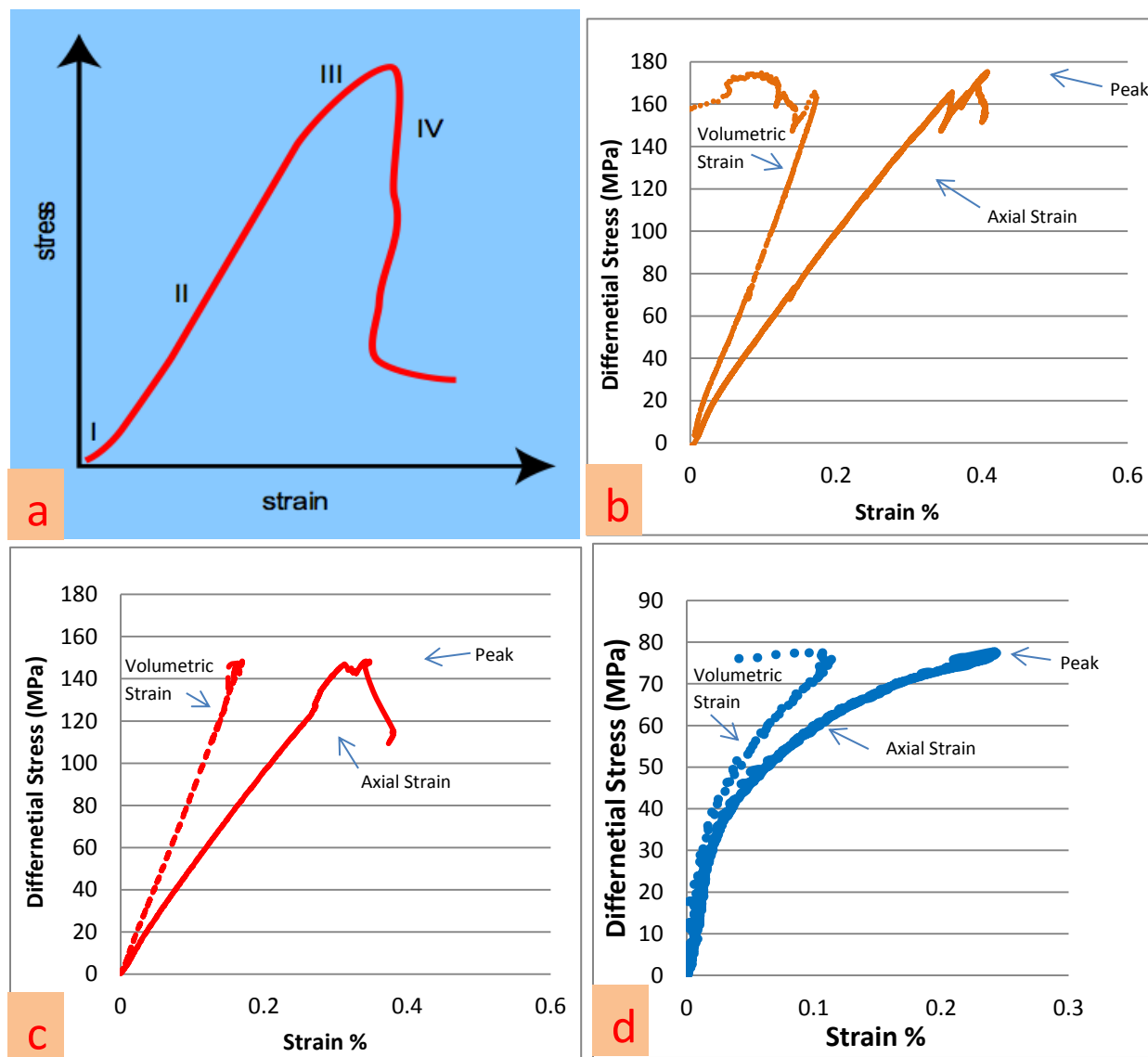


Figure 4. Axial and Volumetric Strain plots for samples S11.3, S11.2 and S11.1: (a) typical curve seen during deformation of materials. Stage I is closure of cracks, stage II is elastic deformation (Young's Modulus), stage III is inelastic deformation, and the final stage is micro-cracks connecting. (b) Plot of S11.3 with axial strain shown with a solid orange line, volumetric strain shown by the dotted orange line, and peak stress pointed to with the arrow. (c) Plot of S11.2 with axial strain shown with a solid red line, volumetric strain shown by the dotted red line, and peak stress pointed to with the arrow. (d) Plot of S11.1 with axial strain shown with a solid blue line, volumetric strain shown by the dotted blue line, and peak stress pointed to with the arrow.

### 4.3 Porosity and Permeability of Deformed Samples

After deformation, the deformed samples were tested for porosity and permeability. The deformed porosity and permeability results yielded only permeability measurements with the new micro-cracks created. Porosity was attempted to be taken but after testing the samples at low confining pressures, not data was able to be acquired. This is possibly due to the confining pressure compressing the sample and closing any cracks. As for permeability, values were able

to be acquired as seen in Fig. 5. Permeability values ranged from 1.3 mD to close to 3.3 mD. This increase in permeability is significant because the undeformed samples had permeability values below .01 mD.

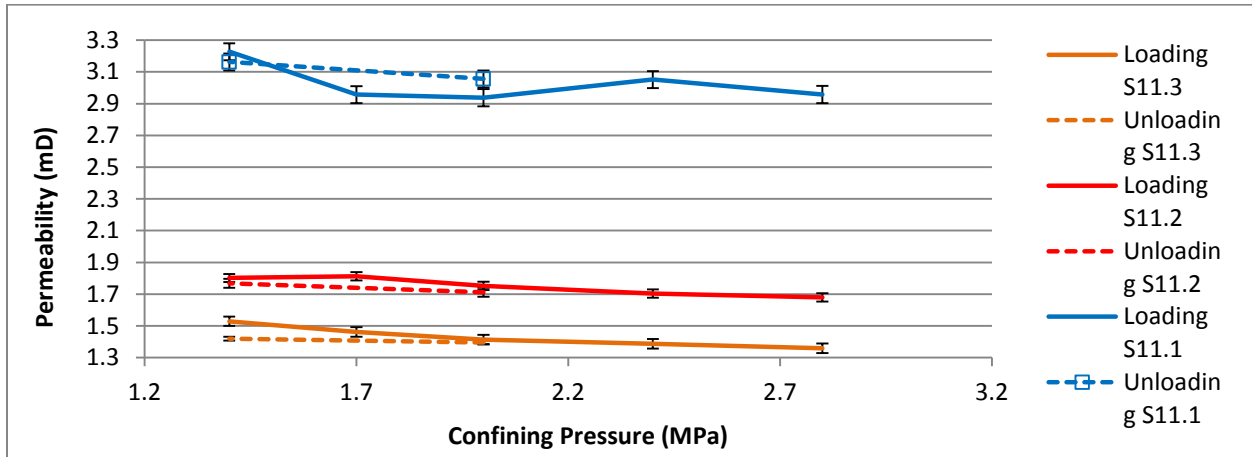


Figure 5. Deformed samples permeability results: Solid lines show loading of confining pressure while dashed lines show unloading of confining pressure. These results were acquired using the Permeameter. Error bars measure within one standard deviation.

#### 4.4 Microstructure Analysis

Visual data from thin sections of undeformed and deformed were analyzed to see visually how mechanically induced stress affected the samples. In Figure 1 (left), a picture of an undeformed sample is shown. A closer look at Figure 1 (left) reveals pre-existing cracks as well as clay material orientation. In Figure 6a, the pre-existing crack can be seen oriented with the bedding planes. Looking at thin section of the bedding parallel sample S11.2, no cracks can be seen by the naked eye. When viewed in the microscope, crack networks propagating vertically are revealed (Fig. 6b). As for the bedding perpendicular sample S11.1, complete failure occurred along with smaller crack networks parallel to the fracture. As seen in Fig 6b and 6c, visible white cracks propagate in the direction of expected bedding laminations.

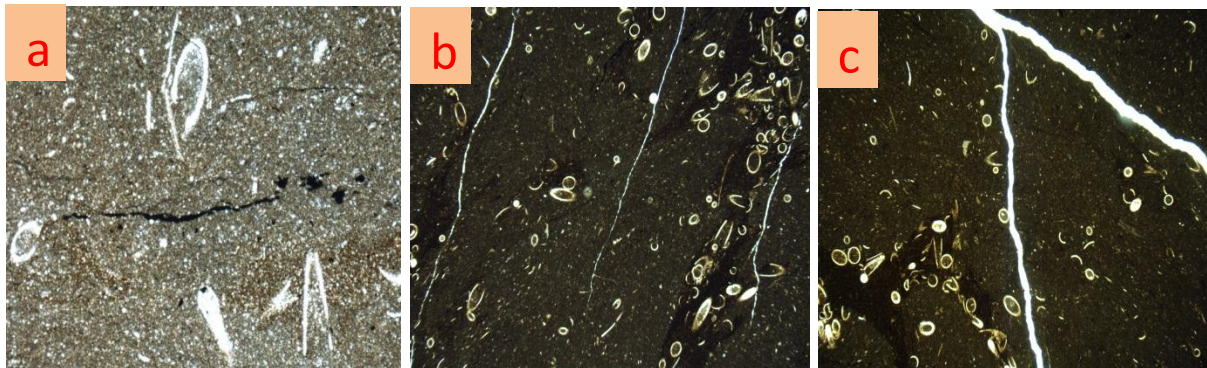


Figure 6. Thin section views of undeformed and deformed samples. (a) zoomed in image of Fig 1 (left) showing the pre-existing crack running along bedding orientation. (b) Sample S11.2 with a visible crack network created parallel to bedding laminations. (c) Sample S11.1 with a fracture running along the expected bedding lamination with a smaller fracturing propagating downward.

## 4.5 Uncertainty

Due to difficulty of obtaining Marcellus Shale cores and the one-time use nature of the samples, the scope of uncertainty during research was a concern. Due to lack of samples, multiple precautions during sample testing and preparation were taken into consideration to obtain the most accurate results. During the measurement of porosity and permeability, multiple tests were conducted at multiple confining pressures. It was done to ensure that there are no leaks around the sample as well as to see if the small amount of increase in the confining pressure impacts the porosity and permeability of the sample. For the initial porosity, seven measurements were taken at each confining pressure to obtain an average percent porosity. For post-deformed permeability results, six measurements were taken as confining pressure was loaded and then retaken as the confining pressure was unloaded. This was done to see if unloading had immediate effects on the sample. Again, at each confining pressure, six measurements were conducted to obtain an average permeability.

Strain gages are used to measure axial and radial change in the samples during deformation. Each gage has thin wires that have a known resistance across an area. The gage experiences deformation, when a force is applied. This is recorded by the small change in resistance on the gage. Each gage was made to have 120 ohms of resistance with +/- 0.5% error. Two different gauges were used; one was only an axial gage, while the other had an axial and a radial gage. For the axial gage, the resistance was 120 +/- 0.3% and for the axial/ radial gage, the resistance was 120 +/- 0.4%. Assuming maximum error, the experiment would be off by +/- 0.11%. The values acquired by the gages are used in the calculation for volumetric strain, which affects deformation plots as well as Poisson's ratio and Young's modulus.

## 5. Discussion

### 5.1 Undeformed Samples

The first tests conducted were the initial porosity and permeability of each sample. The initial porosity results show that there were pore spaces in the pre-deformed sample. Values ranged on average between 0.1% to 0.4% porosity for samples S11.1 and S11.2 (Fig. 3). These values are extremely low but expected when dealing with shale that has low porosity and permeability values. For the sample S11.3, which had bedding parallel to laminations, no porosity measurements could be made. This result indicates that the percent porosity in the sample was below 0.05%. For the initial permeability results, no data could be acquired for any of the samples, which was expected when working with carbonate-rich shale. The lowest possible permeability value that the permeameter can read is  $\sim 10^{-17} \text{ m}^2$  or 0.01 mD.

Observing the pre-deformed thin sections, the black dots and cracks are not open pore spaces. Even though they are not open pore spaces, research done by Ece (1987) have led to the

conclusion that the black cracks (Fig. 1 (left)) were originally open but have been filled in with small silt sized particles. These particles filled in as deposition occurred, which helps identify bedding orientation. The reason for this observation is based on how the black cracks bend around and do not continue through microfossils. In some thin section views, such as Figure 1 (right), a slight discoloration is seen due to multiple types of similar clays being deposited and moved around by microorganisms after deposition. This clay contrast has no definite direction and varies in size and shape throughout the laminations. The pore spaces in most thin sections views of shale samples are on the order of ten to hundred nanometers NETL (2010). Even though pore spaces are small, they still exist and are randomly oriented throughout the sample. In Figure 1a (left), most of the features discussed previously can be seen along with microfossils. Consulting with James E. Day from Illinois State University, the microfossils have been determined to be dacryonarids and small echinoderm stem plants.

## **5.2 Deformation Experiments**

In order to obtain a baseline, as well as perform the first deformation test, the S11.3 sample was used. The S11.3 sample has bedding parallel to laminations and was subjected to 30 MPa confining pressure during the experimental run. The 30 MPa confining pressure was used assuming the sample was going to be saturated. The sample was impervious to all attempts of experimental infiltration with respect to water. During each attempt, axial stress was released and a negative pore pressure was created to pass water through the sample. This is seen on the curve in Figure 4b by a high stress followed by a short fall in stress as the sample settled. At a 30 MPa confining pressure the sample was being exposed to pressures expected at 1.9 km below earth's surface. As seen in Figure 4b, the axial extension curve is behaving as expected with a few high and low marks where permeability measurements were taken. Starting around 120 MPa, the line begins to curve. This means that cracks are beginning to form but have not started connecting. At 177 MPa, peak stress was reached. At this point, stress began to drop meaning the brittle fractures were occurring, which allowed crack networks to form.

The second experimental test was conducted using the second sample (S11.2) taken parallel to bedding planes. After analyzing the baseline experiment, a few parameters were changed to obtain more brittle deformation. Confining pressure was decreased to half the initial pressure and the strain rate was increased by half an order of magnitude. Decreasing the confining pressure would allow more brittle deformation and increasing the strain rate was done to conduct the experiment in a timelier manor. Due to the impervious characteristics of the shale, permeability tests were not attempted during deformation. Comparing Figure 4c to 4b, the curves are just about identical, with peak stress being slightly smaller for the S11.2 sample. The peak stress for S11.2 sample was around 146 MPa, which was expected with the confining pressure being lower.

The final sample taken perpendicular to bedding planes was tested under the exact same parameters as the S11.2 sample. With the expected laminations to be perpendicular to the

maximum principle stress, a few visual observations were made before preparing the sample. As seen in Appendix A, Fig. F, the sample had visibly different clay contrast inside the sediment orientation at a 15 degree angle to the expected bedding planes. In Figure 4d, different results occurred in the deformation data. A few points to emphasize are that crack closure was completed under less stress followed by a shorter elastic deformation stage. This was expected because the bedding planes are being compacted in the way sediments settled. Damage in the sample begins to occur at a lower stress seen in Figure 4d due to the bedding planes already being compacted. As more stress is applied, the dilatancy of the sample begins rapidly increasing. With the crack networks assumed to be harder to create, at only 78 MPa complete failure occurred. This result was not ideal since secondary tests results may have skewed results with a fracture inside the sample.

Young's modulus ( $E$ ) is the measure of the stiffness of a material. For this experiment, Young's modulus shows how much the sample shrinks during compression. Young's modulus is the ratio of the differential stress to the axial strain (Equation 5). Figure 7a-c show Young's modulus for each sample. The Young's modulus range for the samples gets smaller from  $E_3$  to  $E_1$ . As stated previously, from  $E_3$  to  $E_2$  the confining pressure was decreased from 30MPa to 15MPa. This change allowed the sample to expand horizontally easier when subjected to stress. For the change in stiffness from  $E_3$  &  $E_2$  to  $E_1$ , the bedding orientation is perpendicular to bedding planes causing an increase in the stiffness of the sample. The Young's modulus for shale can range depending on composition but on average the value is between 1 and 90 GPa. Looking at Figures 7a-7c, the values obtained are on the lower end. For the two samples bedding parallel, the Young's modulus values were 0.465 GPa and 0.472 GPa. For the sample bedding perpendicular, the value was 1.4 GPa. From Figure 7d, the difference between the two bedding orientation values can be seen graphically being much different. The data results show that the shear strength of the sample bedding perpendicular to laminations was 3 times higher than the samples bedding parallel to laminations. This feature is significant in that the confining pressure and strain rate was the exact same for S11.2 which resulted in 0.472 GPa and for S11.1 which resulted in 1.4 GPa.

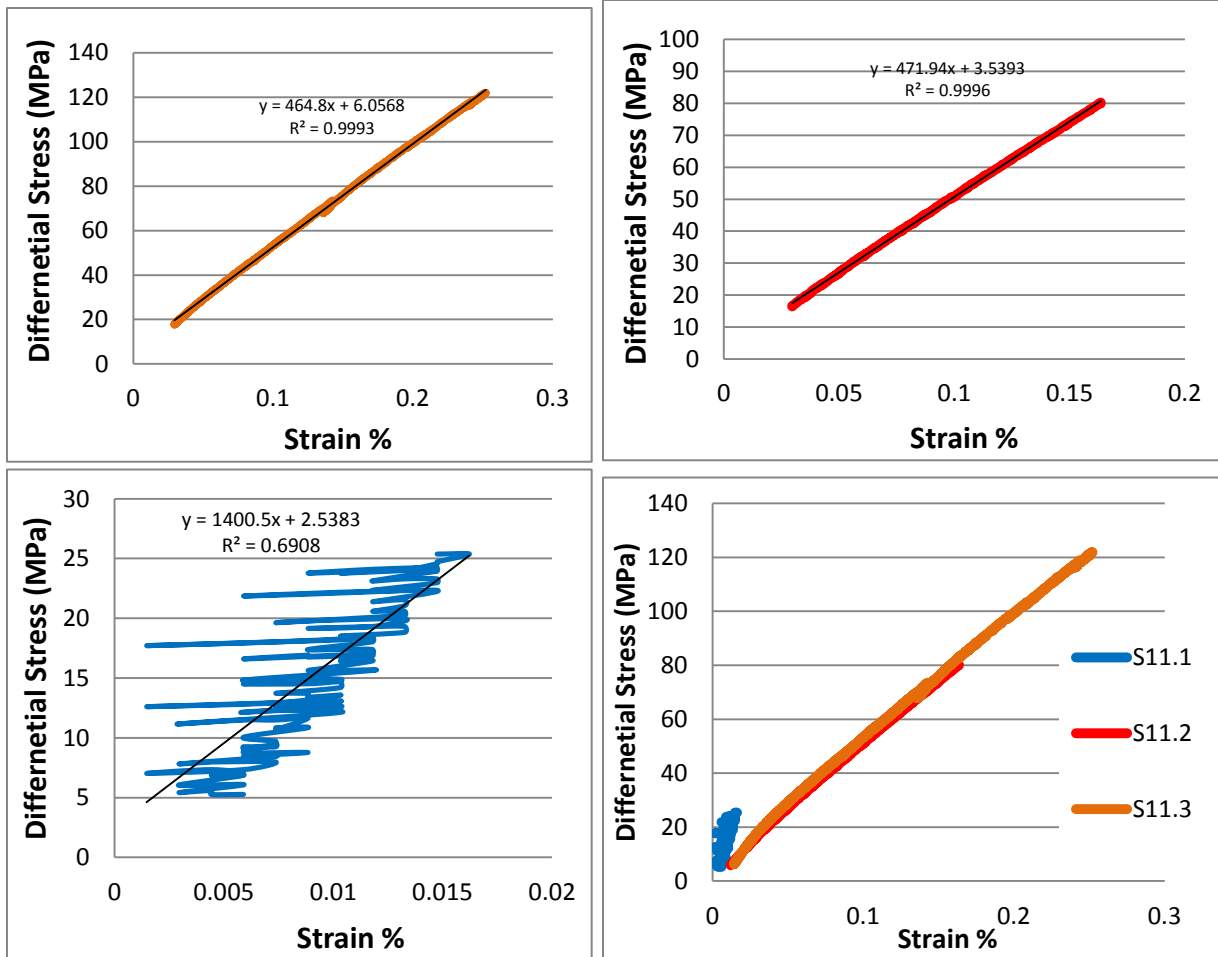


Figure 7. Young's modulus (E) graphs: (a) Graph of  $E_3$  for sample S11.3 showing a value of 0.465 GPa. (b) Graph of  $E_2$  for sample S11.2 showing a 0.472 GPa. (c) Graph of  $E_1$  for sample S11.1 showing a value of 1.4 GPa. (d) Graph comparing each Young's Modulus value. Samples S11.3 and S11.2 were taken parallel to the bedding planes while sample S11.1 was taken perpendicular to bedding planes.

Poisson's ratio is the ratio of radial strain to the axial strain. Shale on average is known to have Poisson ratio values between .2 and .4. For my experimental runs, all three samples had ratios between .24 and .25 (seen in Figs. 8a-8c). This shows that the general compressive nature of each shale sample were the same. Even though the elastic phase of each sample varied, the overall change in the sample had the same reaction during deformation. This similarity can be seen in Figure 8d with each experimental ratio plotted together.



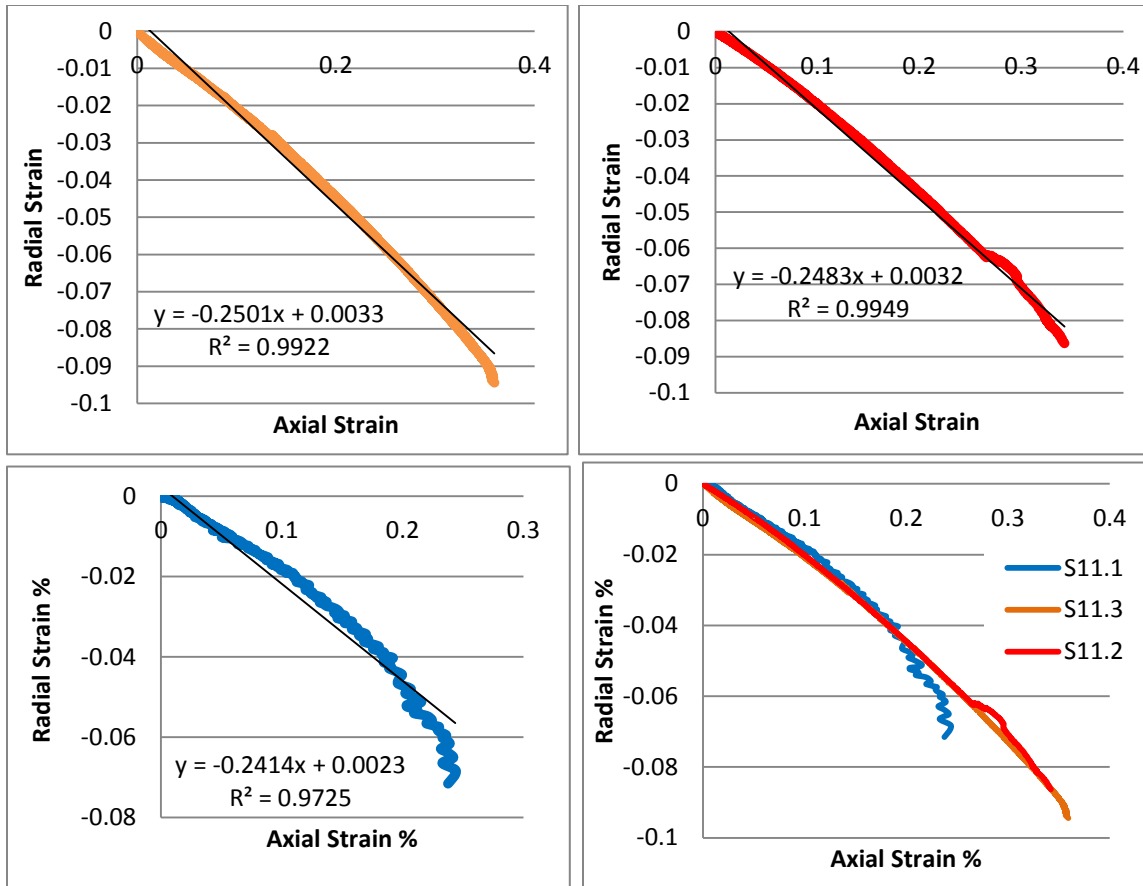


Figure 8. Plot of Poisson's Ratio: Radial strain being on the y-axis and axial strain being on the x-axis (a) Plot of S11.3 showing Poisson's ratio of .25 (b) Plot of S11.2 showing Poisson's ratio of .248 (c) Plot of S11.1 showing Poisson's ratio of .24 (d) Graph of all three samples plotted together.

### 5.3 Deformed Samples

Following deformation, porosity and permeability tests were conducted. For the deformed samples, porosity measurements could not be obtained. This is expected with pore spaces in shale being small and not well connected. With the small confining pressure used during the porosity measurements, possible cracks created during deformation could have closed. Permeability results for the samples could be taken, meaning that micro-cracks created during deformation connected. The newly formed crack networks allow gas to move through the deformed sample. For the samples taken parallel to bedding, the average permeability measurement seen in Figure 5 was between 1.3 mD to 1.9 mD. This is significant, because undeformed permeability results were over two orders of magnitude smaller at less than 0.01 mD (Fig. 9). For final permeability measurements, loading and unloading data was collected to determine if confining pressure affected the results. As seen in Figure 7, the loading of confining pressure causes the permeability to decrease gradually but only by a factor of 0.15 to 0.2 mD. As the confining pressure was released, more measurements were taken showing the permeability was lower than when initial measurements were taken. This is to be expected, as the sample will

elastically expand back to its original shape at a slower rate. In Figure 5, sample S11.1 has a varying loading slope compared to the more gradual change seen by samples S11.3 and S11.2. This is possibly due to the fracture that lies within the S11.1 sample. As the confining pressure was applied, the fracture in the sample gradually closed. Once a confining pressure of 1.5 MPa was reached, the permeability leveled out. The results for sample S11.1 are consistent with the other samples taken parallel to bedding planes in that the permeability was only 1 mD greater. The values for the S11.1 sample are higher than hypothesized but the fracture likely allowed more gas to flow through during the measurement.

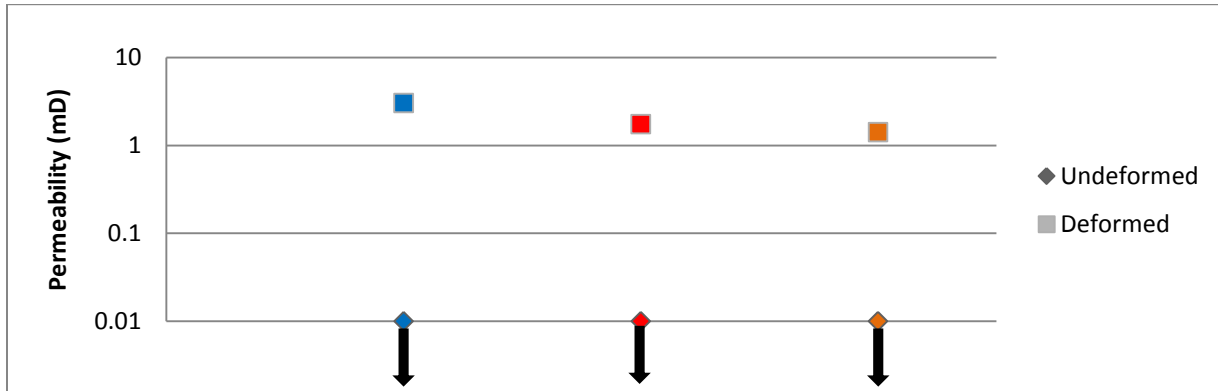
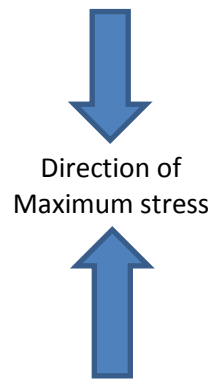
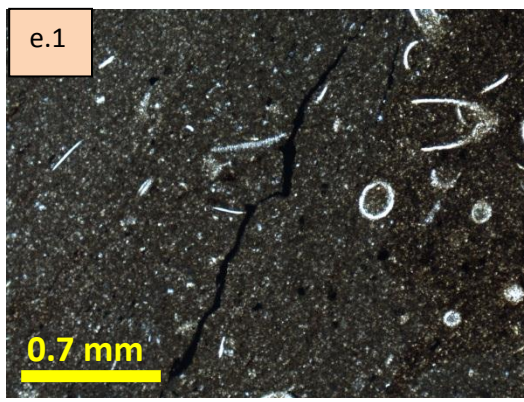
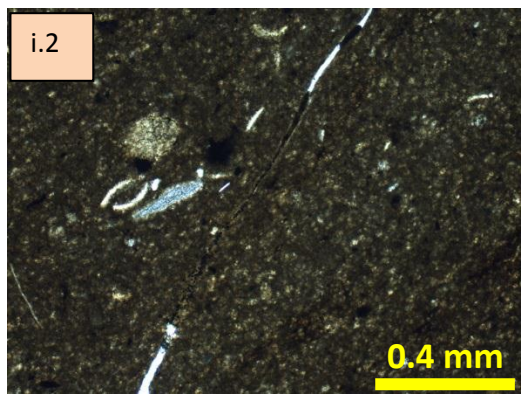
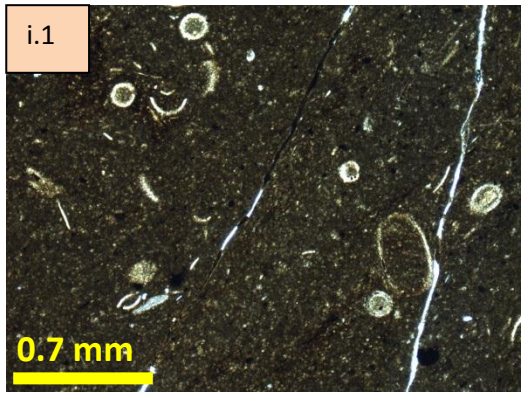
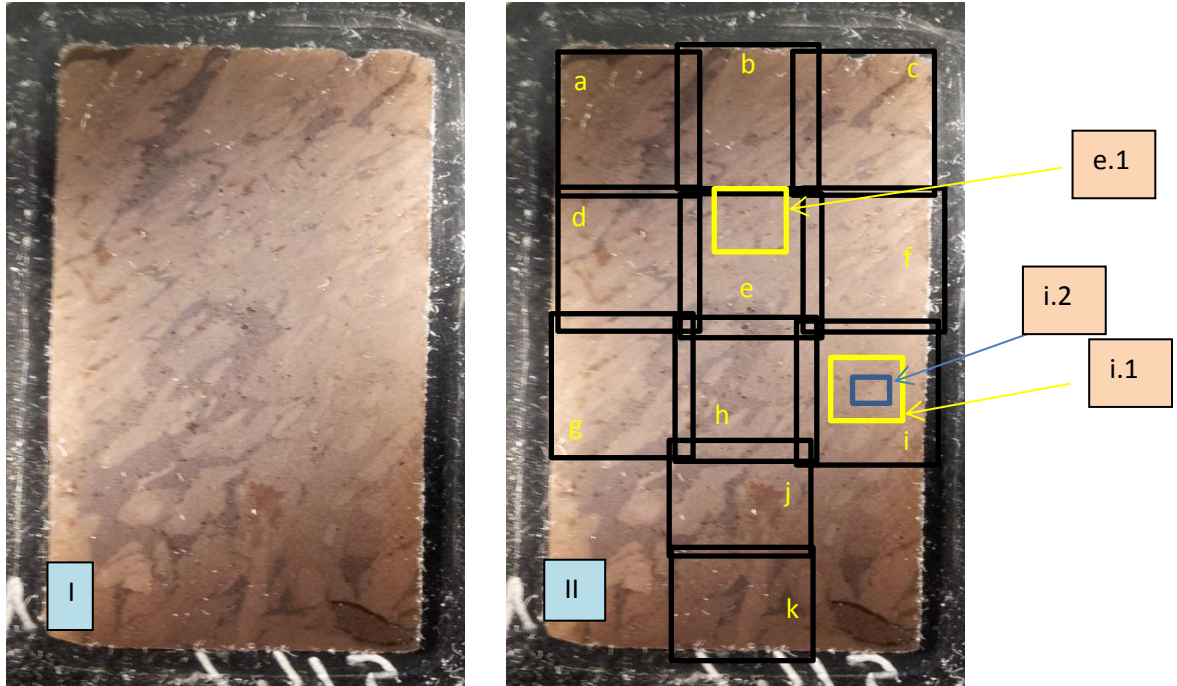


Figure 9. Undeformed permeability compared to deformed permeability results. The solid box represents the values obtained during deformation while the diamond shape with the arrow below represents the maximum value the permeameter can acquire. Blue represents S11.1, red represents S11.2, and orange represents S11.1.

#### 5.4 Microstructure Analysis

The deformed thin sections of the samples reveal the best evidence of how cracks propagated after stress was applied. Multiple cracks occurred in the sample taken parallel to the bedding planes, seen in Figure 10a-k. Throughout the whole thin section, visible cracks happened parallel to the bedding plane. Pre-existing cracks, as seen in Figure 10i.1 and 10i.2, show that some cracks began to open but not completely. Figure 10i.2 shows that the black crack is still visible even though cracks have opened above and below the area. In Figure 10e.1 the general orientation of the samples had pre-existing cracks parallel to the direction of maximum principle stress. The crack networks created formed in the exact orientation as pre-existing cracks that did not open. With black cracks defining lamination, crack networks formed along the shale laminations.



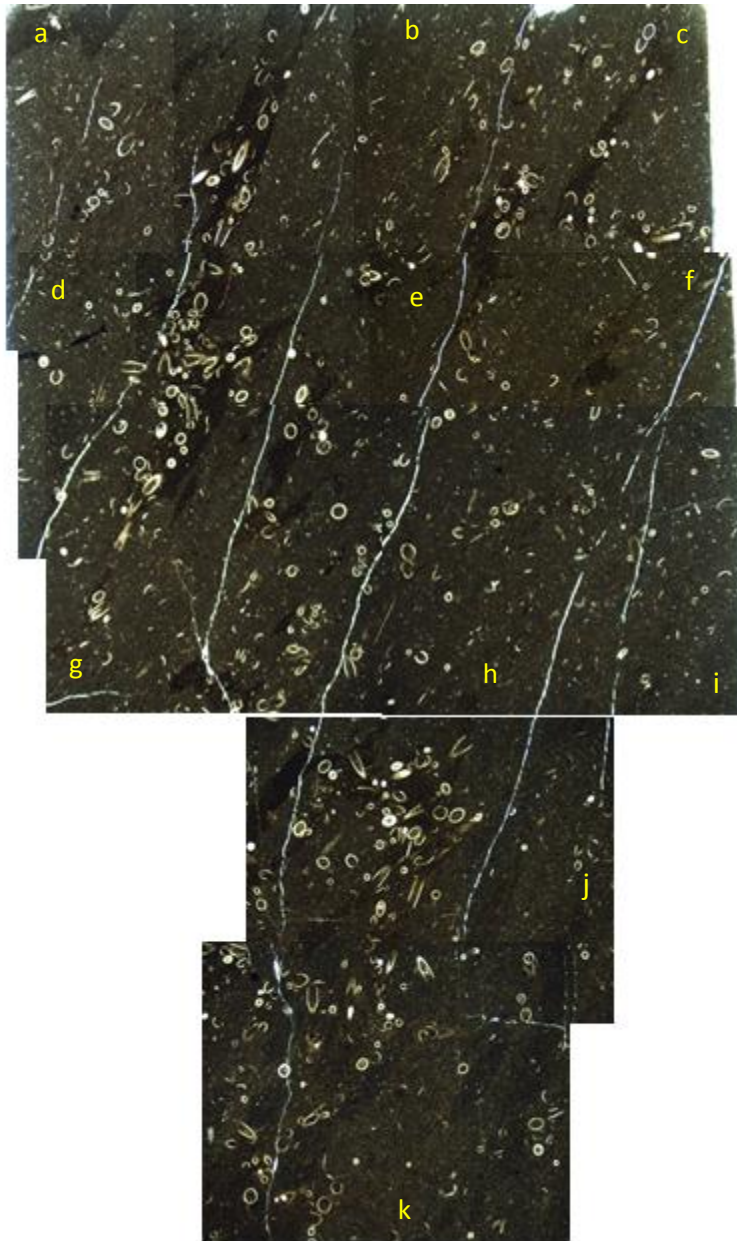
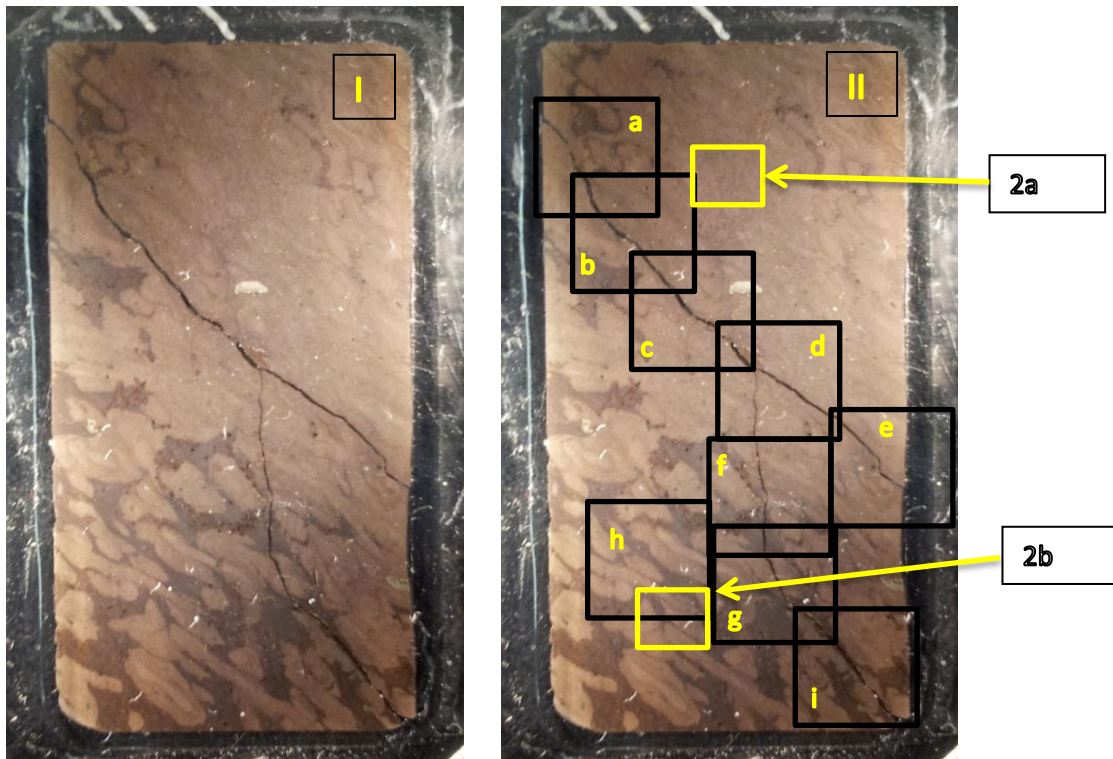
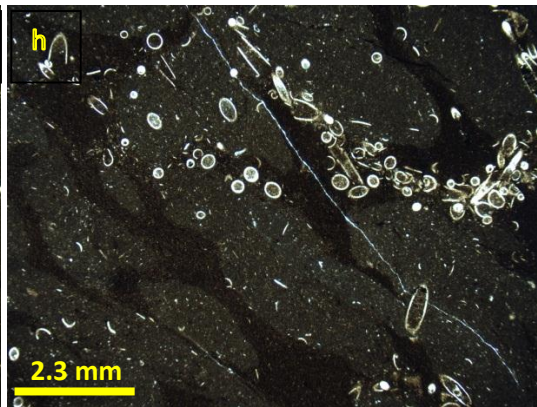
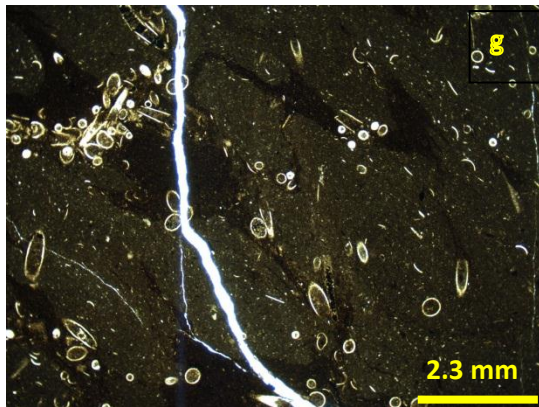
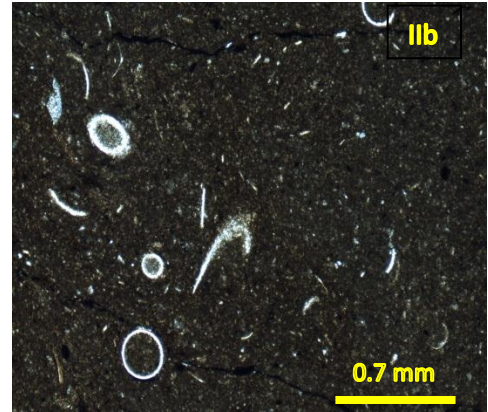
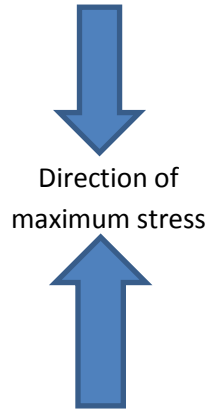
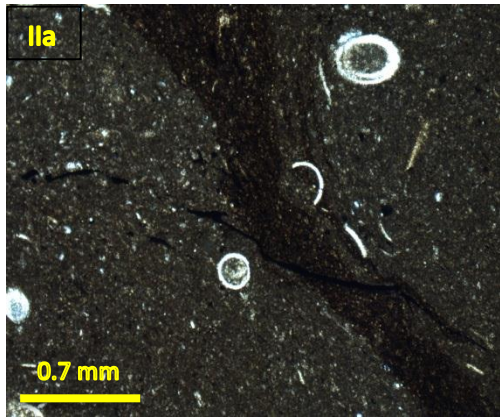


Figure 10. Deformed S11.2 thin section: I is a picture of the thin section from deformed S11.2 sample. After deformation the sample was cut perpendicular to the fracture axis for the thin section to be made. From the image II, black boxes show where on the thin section each smaller image was taken from. (a-k) Images that have been taken at 1.5x zoom using a photomicroscope and made into a mosaic. From this mosaic multiple cracks can be seen created vertically due to deformation. Also seen in every thin section are micro-fossils as well as different colored clays that make up the shale rock. (i.1) Image taken at 5 times zoom to show the white lines are new cracks and black lines are pre-existing cracks. (i.2) Image taken at 10 times zoom to show the white lines are new cracks and black lines are pre-existing cracks.

As for the S11.2 sample (Fig. 11.1), complete failure occurred, which is visible by the large fracture. Even though complete failure occurred, this sample produced an interesting crack network. Before the sample was prepared for deformation, a visible clay mineral contrast angle inside the sediment orientation could be seen. From Figure 11.1, a small fracture occurred at a 45 degree angle above the clay contrast area. Figures 11.2a and 11.2b both show pre-existing cracks that did not open, Figure 11.2a showing a pre-existing crack above and Figure 11.2b being below the fracture. These pre-existing cracks run perpendicular to the direction of maximum stress and parallel to the crack networks created. Not only is there a complete failure along this orientation, we also see a small fracture occur below the main fracture. In Figure 11g, the secondary fault is seen dropping vertically down and then dipping off to the right. At this point, the larger fracture drops to the right but a smaller crack is seen going upward and to the left in the sample. Looking more closely at the section 11g, the crack seems to separate at two clay mineral boundaries. This could be possible due to the clay mineralogy structure being a defect in the shale. This characteristic is then seen again as small crack proceeds to break away and continue into region of more clay variations. In figure 11h, the crack continues to propagate and at certain points seems to propagate along the clay mineral boundaries.





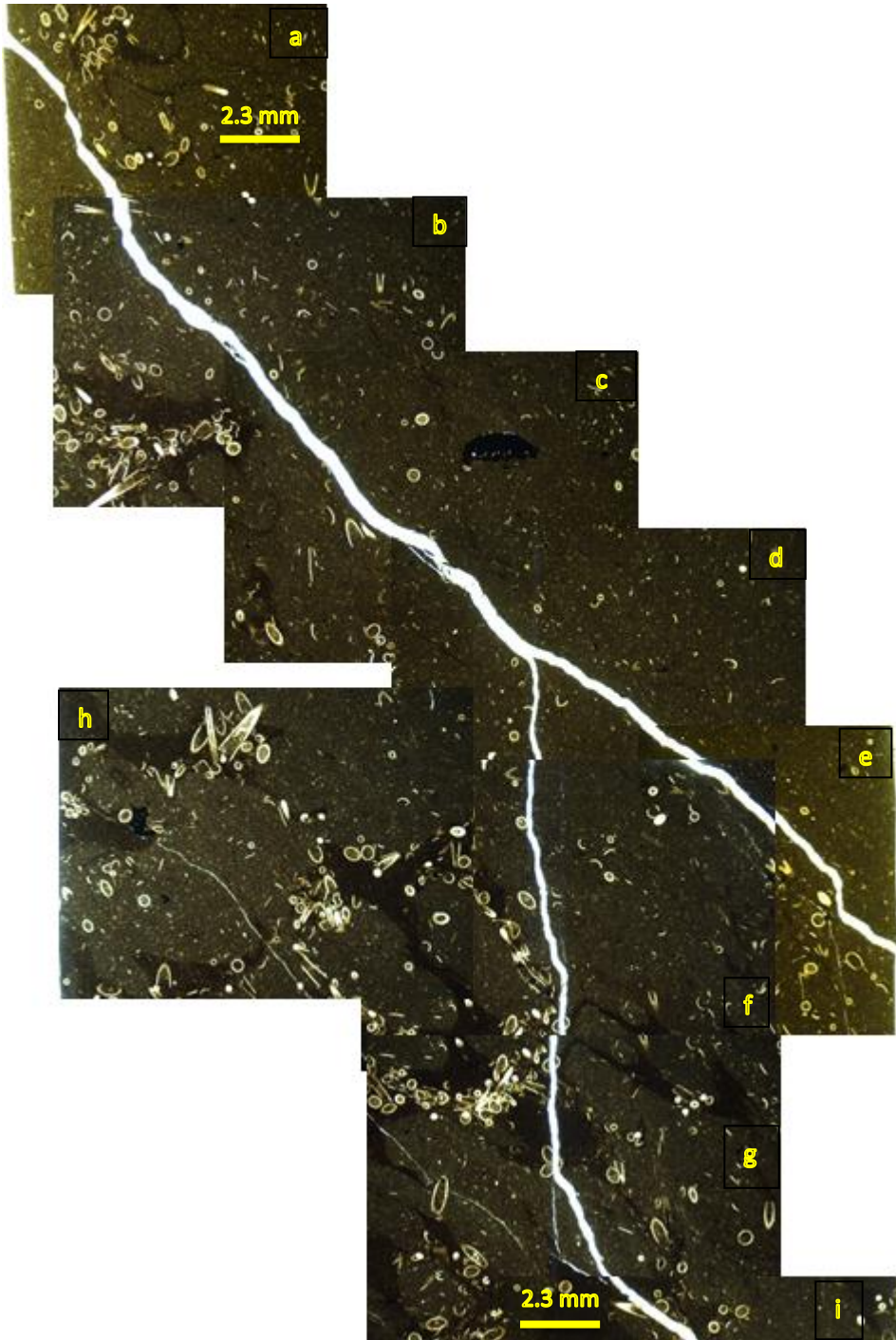


Figure 11. Deformed S11.1 thin Section: Image I is a picture of the thin section from deformed S11.1 sample. After deformation the sample was cut perpendicular to the fracture axis for the thin section to be made. From the image II, black boxes show where on the thin section each smaller image was taken from. (a-i) Images that have been taken at 1.5x zoom using a photomicroscope. White lines represent new cracks created during deformation. During deformation a complete fracture occurred seen by the wide white line. From image 1, clay deposits dip to the right at around a 30 degree angle. A point to make known is the fracture happened parallel to the dipping clay mineralogy. (IIa) Image of a pre-existing crack above the fracture running perpendicular to maximum principle stress direction. (IIb) Image of a pre-existing crack below the fracture running perpendicular to maximum principle stress direction.

## **Future Work**

Shale formations all over the world are becoming relevant due to the economic potential imbedded within. Better understandings of how bedding planes or planes of weakness affect the formations can result in more efficient extraction of the gases it holds. Despite very limited amount of samples and major constraints on available previous research, this thesis project obtained great results. With that in mind, there is still more work that can be done.

Obtaining samples of shale may be difficult due to the depth of formations, but with multiple samples the results can be better compared. A future study could involve not only collecting cores again at perpendicular and parallel to bedding planes but also at multiple angles in between such as 15, 30, 45, 60, and 75 degrees. A major factor in obtaining the best results is the prevention of complete failure during deformation. A secondary part of that research is to obtain the multiple samples from different parts of a shale formation due to varying shale features, gas levels and mineral characteristics. A similar method of analysis can be used to obtain results that would be influential to future shale structure research.

## **Conclusion**

In this study, I conducted deformation tests and microstructural analysis to characterize the effect of bedding laminates on crack propagation in anisotropic Marcellus shale samples. Key observations are summarized below:

1) Shear strength and elastic moduli of the Marcellus Shale samples depend strongly on bedding laminates. At the same confining pressure and strain rate, the deformation data show that the shear strength of the bedding parallel sample S11.2 is only  $\sim 1/3$  of that of the bedding perpendicular sample S11.1.

2) Crack growth in the deformed Marcellus Shale samples is controlled by the interplay between stress, bedding laminates, as well as the silt-clay strength contrast within the sedimentary layers. The stress-induced cracks are generally subparallel to the maximum principal stress. Changes in crack orientation are observed along bedding laminates and clay minerals.

3) Comparison of the permeability values of the deformed samples to those of the undeformed samples indicates that stress-induced crack growth enhances permeability of the shale.



## **Acknowledgements**

I would first like to thank Wen-lu Zhu for the being my advisor for the past nine months. With her help I was able to learn the necessary material required for this senior thesis research. I would also like to thank post doctorate and graduate students Audrey Ougier-Simonin, Harry Lisabeth and Jeremy Banker for help in sample preparations and more importantly training me on the triaxial deformation apparatus, porosimeter and the permeameter. I would like to thank Palma Botterell for providing me with my Marcellus Shale sample. Finally, I would also like to thank the University of Maryland, Department of Geology for allowing me to use the available resources to accomplish this senior thesis.

## References:

- Li, Yawei and Ghassemi, and Ahmad. Creep Behavior of Barnett, Haynesville, and Marcellus Shale. Thesis. Texas A&M University, 2012. N.p.: American Rock Mechanics Association, n.d. Print.
- Soeder, Daniel J., and William M. Kappel. "Water Resource and Natural Gas Production from the Marcellus Shale." USGS (2009): n. pag. Print.
- Crawford, B. R., N. L. DeDontney, B. Alramahi, and S. Ottesen. Shear Strength Anisotropy in Fine-grained Rocks. Thesis. Houston Texas, 2012. N.p.: American Rock Mechanics Association, n.d. Print.
- Sondergeld, C.H. and C.S. Rai. 2011. Elastic anisotropy of shale. The Leading Edge March 2011.
- Soeder, Daniel J. "The Marcellus Shale: Resources and Reservations." EOS, Transactions, American Geophysical Union 91.32 (2012): 277-88. Print.
- Gribbin, J. L., W. Zhu, and M. K. Tivey (2012), Anisotropy in seafloor flange, slab, and crust samples from measurements of permeability and porosity: Implications for fluid flow and deposit evolution, *Geochem. Geophys. Geosyst.*, 13, Q03018, doi:10.1029/2011GC003840.
- Randall, C.J. "The Impact of Marcellus Gas Drilling on Rural Drinking Water Supplies by the Center for Rural Pennsylvania, March 2012." Scribd. N.p., Mar. 2012. Web. 18 Oct. 2012. <<http://www.scribd.com/doc/86242795/The-Impact-of-Marcellus-Gas-Drilling-on-Rural-Drinking-Water-Supplies-by-the-Center-for-Rural-Pennsylvania-March-2012>>.
- Delle Piane, Claudio, D. N. Dewhurst, A. F. Siggins, and M. D. Raven. "Stress-induced Anisotropy in Brine Saturated Shale." *Geophysical Journal International* 184.2 (2011): 897-906. Print.
- Milner, M., R. McLin, and J. Petriello. "Document Preview." *Imaging Texture and Porosity in Mudstones and Shales: Comparison of Secondary and Ion-Milled Backscatter SEM Methods*. Society of Petroleum Engineers, 2010. Web. 15 Nov. 2012. <<http://www.onepetro.org/mslib/servlet/onepetropreview?id=SPE-138975-MS>>.
- Robinson. "Reducing Environmental Risk Associated with Marcellus Shale Gas Fracturing." *Oil & Gas Journal* 110.4 (2012): 88-91. Print.
- Snow, Nick. "Producers, Regulators Address Marcellus Shale Gas Challenges." *Oil & Gas Journal* 106.42 (2008): 24-26. Print.

"Impact of the Marcellus Shale Gas Play on Current and Future CCS Activities." National Energy Technology Laboratory (2010): n. pag. Print.

Ece, Omer I. PETROLOGY OF THE DESMOINESIAN EXCELLO BLACK SHALE OF THE MIDCONTINENT REGION OF THE UNITED STATES. Thesis. University of Tulsa, 1987. N.p.: n.p., n.d. <<http://www.clays.org/journal/archive/volume%2035/35-4-262.pdf>>

Schieber, Jurgen. "Miscellaneous Sedimentary Feature." Miscellaneous Sedimentary Featur. IU Bloomington Department of Geosciences, 10 Dec. 2006. Web. 5 Apr. 2013.

"A Comparative Study of the Mississippian Barnett Shale, Fort Worth Basin, and Devonian Marcellus Shale, Appalachian Basin." National Energy Technology Laboratory, Apr. 2011. Web. Dec. 2012.

Olmstead, Sheila A., Lucija A. Muehlenbachs, Jhih-Shyang Shih, Ziyan Chu, and Alan J. Krupnick. "Shale Gas Development Impacts on Surface Water Quality in Pennsylvania." Shale Gas Development Impacts on Surface Water Quality in Pennsylvania. N.p., 8 Jan. 2013. Web. 30 Mar. 2013.

## Appendix

### Appendix A: Figures

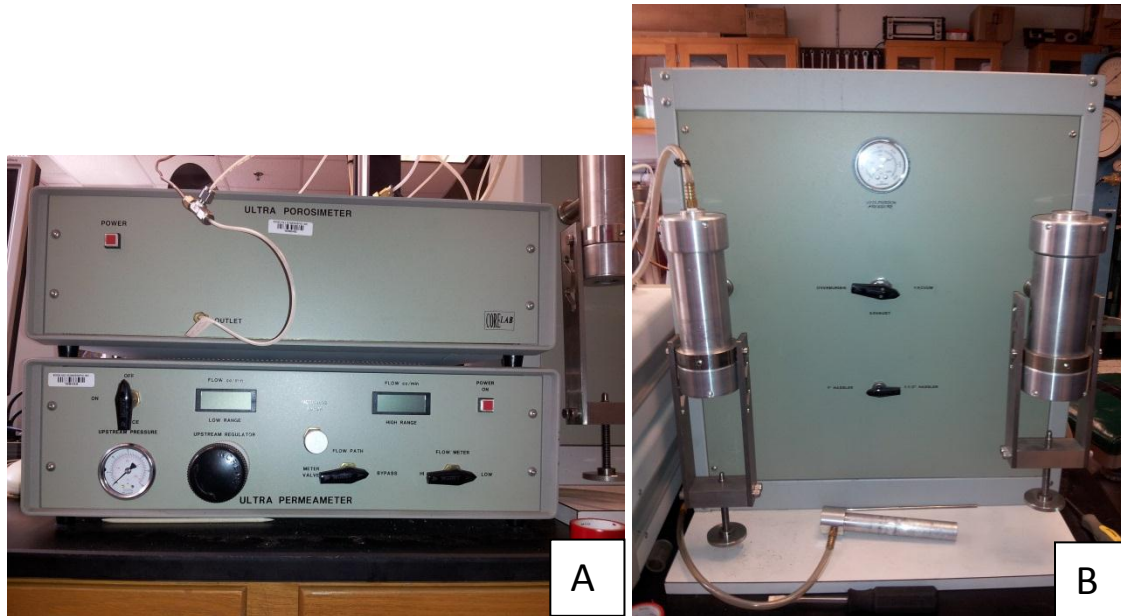


Figure A & B: Experimental testing machines: (A) image of the Porosimeter on top and the Permeameter on the bottom. These two machines use helium and nitrogen respectively to test sample porosity and permeability. (B) image of the testing chambers where samples are inserted and sealed for gas to flow into or thru depending on the test being done.



Figure C: Triaxial deformation apparatus: AutoLab 1500

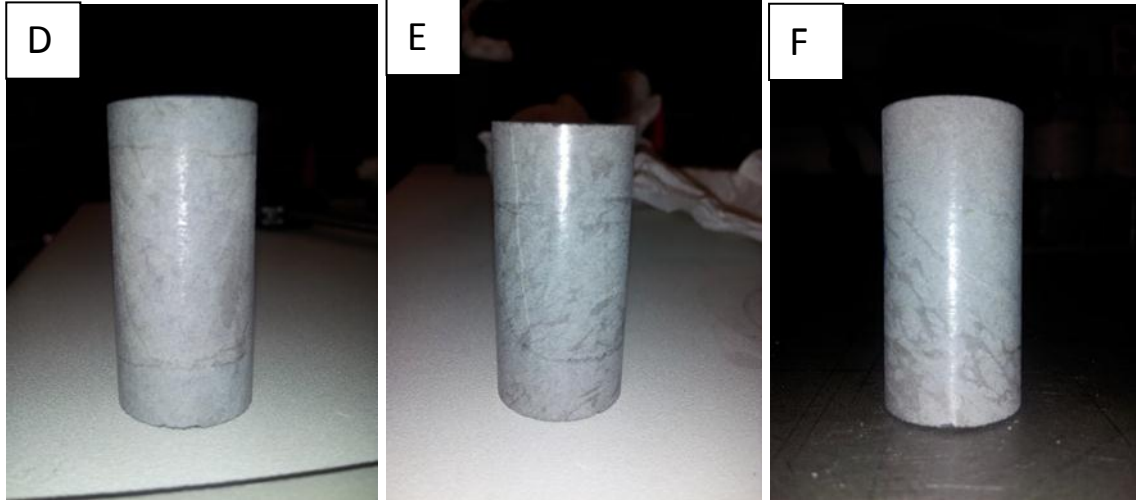
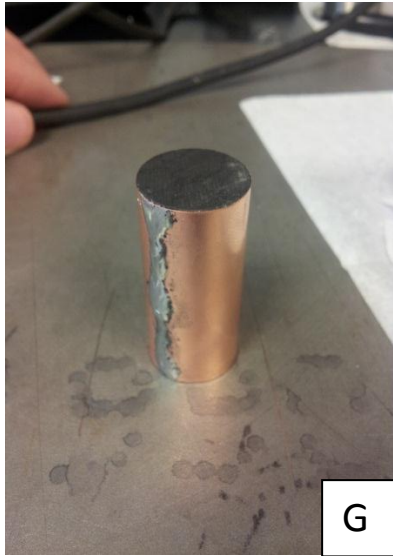


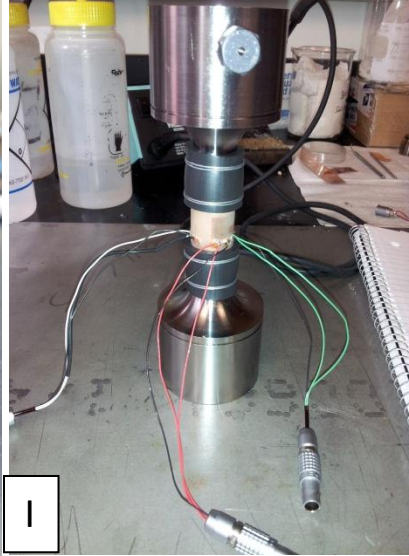
Figure D-F. Undeformed core samples: (D) picture of the S11.3 sample (E) picture of the S11.2 sample (F) picture of the S11.1 sample. Samples S11.2 and S11.3 were taken parallel to bedding planes and sample S11.1 was taken perpendicular to bedding planes. Visually a dark and light gray color variation is seen. This is due to the different clay minerals mixing throughout the original shale formation.



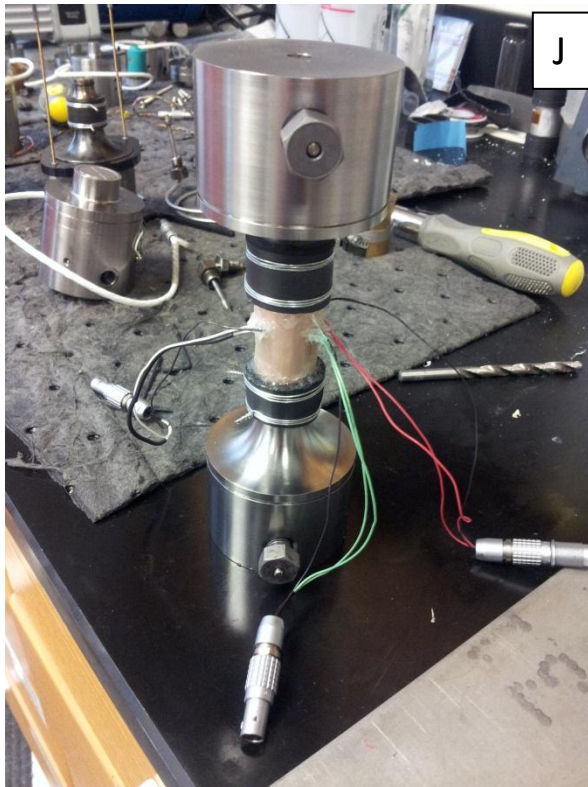
G



H



I



J

Figures G-J. #. (G) picture of a core with the copper jacket soldered on. (H) image of the sample after the axial strain gage has been glued onto the roughened copper surface. (I) image of the core that has been placed onto core mounts. This image also shows the strain gages attached to wires which allow the computer to monitor the sample during deformation. (J) picture of the sample fully assembled with Silicon glue applied to prevent oil from the confining pressure to enter into the sample during deformation.

## Appendix B: Equations

Equation 1. Porosimeter measurements (Helium)

$$\text{Ideal Gas law: } p_1 * V_1 = p_2 * V_2$$

Equation 2. Permeameter measurements (Nitrogen)

$$\text{Darcy's Law: } q = (-k/\eta) * \Delta p$$

Equation 3. Confining Pressure ( $P_c$ )

$$P_c = \rho * g * d$$

Equation 4. Volumetric Stress ( $\sigma_v$ )

$$\sigma_v = \sigma_A + (2 * \sigma_R)$$

Equation 5. Young's Modulus ( $E$ )




$$E = \sigma_D / \epsilon_A$$

Equation 6. Poisson's Ratio ( $\nu$ )

$$\nu = - \epsilon_R / \epsilon_A$$

## Appendix C: Tables

Table 1: Summary of the experiment

Sample Status	Tests	Sample S11.1 (bedding perpendicular) 	Sample S11.2 (bedding parallel) 	Sample S11.3 (bedding parallel) 
Undeformed	Micro-structural Analysis	√	√	√
	Initial Porosity ( $\Phi$ )	√	√	√
	Initial Permeability (k)	√	√	√
	Deformation Test	√	√	√
Deformed	Micro-structural Analysis	√	√	√
	Porosity ( $\Phi$ )	√	√	√
	Permeability (k)	√	√	*

√: Test completed

\*: Not conducted

Table 2: Porosity data of undeformed samples

S11.1 undeformed		Length= 3.828 cm		Diameter= 1.843						
Perpendicular to bedding										
Test #	1	2	3	4	5	6	7	Average	SD	
Confining Pressure (MPa)	porosity %	porosity %	porosity %	porosity %	porosity %	porosity %	porosity %	porosity %	porosity %	
2	0.453	0.232	0.21	0.115	0.21	0.306	0.21	0.248	0.106	
2.4	0.232	0.136	0.306	0.136	0.21	0.38	0.188	0.227	0.089	
2.8	0.284	0.328	0.246	0.401	0.328	0.092	0.188	0.267	0.102	
3.1	0.115	0.115	0.118	0.159	0.284	0.115	0.284	0.170	0.079	
								Average	0.228	0.094
S11.2 undeformed		Length= 3.802		Diameter= 1.844						
Parallel to bedding										
Test #	1	2	3	4	5	6	7	Average	SD	
Confining Pressure (MPa)	porosity %	porosity %	porosity %	porosity %	porosity %	porosity %	porosity %	porosity %	porosity %	
2	0.263	0.286	0.093	0.189	0.263	0.093	0.189	0.197	0.080	
2.4	0.167	0.189	0.263	0.071	0.167	0.338	0.145	0.191	0.086	
2.8	0.145	0.145	0.123	0.123	0.123	0.145	0.145	0.136	0.012	
3.1	0.145	0.263	0.263	0.145	0.338	0.071	0.145	0.196	0.094	
								Average	0.180	0.068



Table 3: Physical properties of samples

	<b>Sample S11.1</b>	<b>Sample S11.2</b>	<b>Sample S11.3</b>
<b>Experimental Condition's</b>	Confining Pressure: 15MPa Strain Rate: $5 \times 10^{-6} \text{ s}^{-1}$	Confining Pressure: 15MPa Strain Rate: $5 \times 10^{-6} \text{ s}^{-1}$	Confining Pressure: 30MPa Strain Rate: $1 \times 10^{-6} \text{ s}^{-1}$
<b>Peak Stress</b>	78 MPa	146 MPa	177 MPa
<b>Young's Modulus (<math>E</math>)</b>	1.4 GPa	0.472 GPa	0.465 GPa
<b>Poisson's Ratio (<math>\nu</math>)</b>	0.2414	0.248	0.25
<b>Undeformed Porosity (<math>\Phi</math>)</b>	Average: 0.228% Standard Deviation: 0.094	Average: 0.180% Standard Deviation: 0.068	Too Low
<b>Deformed Permeability (k) [1 mD= <math>1 \times 10^{-15} \text{ m}^2</math>]</b>	Average: 3.05 mD Standard Deviation: 0.18	Average: 1.747 mD Standard Deviation: 0.04	Average: 1.424 mD Standard Deviation: 0.04

Table 4: Deformed permeability data

S11.3 Deformed							
Test #	1	2	3	4	Average	SD	
Confining Pressure (MPa)	mD	mD	mD	mD	mD	mD	mD
1.4	1.55	1.608	1.485	1.475	1.5295	0.062002688	
1.7	1.506	1.445	1.474	1.423	1.462	0.036009258	
2	1.418	1.415	1.389	1.436	1.4145	0.019364917	
2.4	1.384	1.362	1.389	1.412	1.38675	0.020516254	
2.8	1.358	1.296	1.393	1.392	1.35975	0.045507325	
2	1.396	1.377	1.395	1.412	1.395	0.014306176	
1.4	1.439	1.444	1.346	1.45	1.41975	0.049371888	
					1.423892857	0.035296929	
S11.2 Deformed							
Test #	1	2	3	4	5	Average	SD
Confining Pressure (MPa)	mD	mD	mD	mD	mD	mD	mD
1.4	1.842	1.877	1.823	1.796	1.707	1.809	0.064191121
1.7	1.86	1.825	1.792	1.732	1.806	1.803	0.047180504
2	1.737	1.825	1.726	1.726	1.735	1.7498	0.042340288
2.4	1.735	1.732	1.709	1.699	1.64	1.703	0.038360136
2.8	1.686	1.652	1.678	1.699	1.714	1.6858	0.023306651
2	1.655	1.683	1.713	1.763	1.729	1.7086	0.041602885
1.4	1.806	1.737	1.775	1.83	1.736	1.7768	0.041637723
						1.748	0.042659901
S11.1 Deformed							
Test #	1	2	3	4	5	Average	SD
Confining Pressure (MPa)	mD	mD	mD	mD	mD	mD	mD
1.4	2.913	3.492	3.138	3.241	3.349	3.2266	0.218986986
1.7	3.09	2.834	3.115	3.206	2.538	2.9566	0.271727437
2	3.168	2.451	3.1	3.111	2.854	2.9368	0.297191352
2.4	3.173	2.858	3.149	2.989	3.088	3.0514	0.129372717
2.8	2.914	2.851	3.146	3.021	2.856	2.9576	0.125599761
2	3.053	3.037	3.192	2.905	3.091	3.0556	0.103550954
1.4	3.227	3.199	3.176	3.194	3.015	3.1622	0.084295314
						3.049542857	0.175817789

1 Green numbers mean confining pressure was being loaded

2 Red numbers mean confining pressure was being unloaded

Appendix D. Honor Code

I pledge on my honor that I have not given or received an unauthorized assistance on the assignment.

X \_\_\_\_\_